Computationally Efficient Simulation of Underwater Acoustic Communication systems

Parastoo Qarabaqi, Yashar M. Aval, and Milica Stojanovic
Department of Electrical and Computer Engineering
Northeastern University
Boston, Massachusetts 02115
Email: {qarabaqi, millitsa}@ece.neu.edu, aval.y@husky.neu.edu

***Abstract*—We propose a statistical model for underwater acoustic channel simulation which addresses acoustic propagation laws as well as fading. The fading effects are studied on small-scale (involving distances on the order of the wavelength) and large-scale (due to location uncertainty). These effects are caused by various phenomena such as scattering, system motion and changing environmental conditions, and result in the variation of the instantaneous channel response as well as the average signal to noise ratio. We compare the simulator with real underwater acoustic data obtained during the Kauai Acomms MURI (KAM'11) experiment which was held in July 2011. Simulated and experimental channels exhibit complex Gaussian path fading with a Bessel-type time-correlation on the small scale, and log-normal distribution with an exponentially decaying time-correlation on the large scale. MSE performance is compared for coherent and differentially coherent detection of experimental and simulated data.**

I. Introduction

Underwater Acoustic (UWA) communication systems have to be designed to operate in channels that vary with time as a result of the changes in system geometry and environmental conditions. To facilitate system design prior to deployment, testing can be carried out via simulation. One approach to designing a channel simulator is to repeatedly run deterministic propagation modeling tools such as the Bellhop beam tracing [1] for varying channel conditions, e.g. [2], [3]. Considering the fact that beam tracing tools operate on a single frequency and a fixed geometry, this approach requires numerous executions to cover a typical system bandwidth at sufficient time resolution, which is computationally demanding. A more efficient algorithm, the Virtual Timeseries EXperiment (VirTEX) code [4], has recently been introduced which operates by tracing multiple inter-related beams to assess the cumulative effect on a signal of a given frequency. The computational complexity issue is not completely resolved in this method as it still requires many executions of the Bellhop. Another approach is to use statistical channel models to directly generate the fluctuations that appear on top of the nominal channel. Beam tracing (or similar deterministic) tools are now needed to generate the nominal channel only. This approach was taken in [5] to simulate the large-scale path loss. While that study focused on a specific aspect of the UWA channel, a general simulator has to address both large- and small-scale effects and describe the complete channel impulse response.

A statistical channel model was previously proposed in [6]. This model takes into account the physical aspects of acoustic propagation as well as the effects of inevitable random channel variations. The model distinguishes two types of channel variations based on the space and time scales of the underlying displacements. Large-scale variations are modeled as a consequence of system displacements that cannot be predicted due to uncertainty about the exact system geometry. Once a particular large-scale displacement is given, additional small-scale variation will occur in the path gains and delays. This variation is modeled as a consequence of scattering and motion. Small-scale variations influence the instantaneous channel response, and consequently the instantaneous signal-to-noise ratio (SNR). As such, they are meaningful for the analysis of signal processing algorithms and network protocols, and the assessment of average bit error rate or packet error rate, conditioned on a particular large-scale realization. In contrast, large-scale variations influence the SNR through its local average, causing it to vary over longer periods of time. As such, they are meaningful for the analysis of top-level system functions such as power allocation and the assessment of outage probabilities and statistical coverage.

In this paper, we use the model proposed in [6] to design a channel simulator. The accuracy of the simulator is tested by (i) comparison of the statistics of the simulated channel with those of an actual UWA channel measured during an acoustic experiment, and (ii) comparison of the performance of an UWA communication system operating on the simulated channel and the experimental channel.

The rest of the paper is organized as follows. In Sec. II, the channel model is briefly discussed. The simulated channel is compared against an experimental channel in Sec. III, and the corresponding performance of a system based on Orthogonal Frequency Division Multiplexing (OFDM) with coherent and differentially coherent detection is shown. Conclusions are summarized in Sec. IV.

II. The channel model

A multipath UWA channel is described by path gains h_p and path delays τ_p. In addition, if scattering occurs along the propagation paths, it causes each path to be split into a number of micro-paths with amplitudes $h_{p,i}$ and delays $\delta\tau_{p,i}$.

We define the scattering coefficient as

$$\gamma_p(f,t) = \frac{1}{h_p}\sum_{i=0}^{S_p} h_{p,i} e^{-j2\pi f \delta\tau_{p,i}(t)} \quad (1)$$

The overall channel transfer function is now given by

$$H(f,t) = \bar{H}_0(f)\sum_p h_p \gamma_p(f,t) e^{-j2\pi f \tau_p} \quad (2)$$

where $\bar{H}_0(f)$ is the nominal transfer function of the direct path. The multipath parameters h_p and τ_p may also vary with time, but on a larger time scale, which will be discussed later in this section. Assuming that the number of micro-paths in (1) is sufficiently large, e.g. 10 or more, and that they are independent and identically distributed, the small-scale coefficient $\gamma_p(f,t)$ is modeled as complex Gaussian with mean $\bar{\gamma}_p(f)$ and variance $2\sigma_p^2(f)$.

Assuming that the reflection points of different paths are sufficiently far apart, the paths exhibit uncorrelated scattering. If the probability density function (p.d.f.) and the power spectral density (p.s.d.) of the intra-path delays are known, the time-frequency-correlation function $C_{\gamma_p}(\Delta f, \Delta t)$ of the small-scale coefficient can be obtained. As a special case, this function is analytically derived assuming that the intra-path delays $\delta\tau_{p,i}(t)$ are zero-mean, Gaussian distributed with variance $\sigma^2_{\delta p}$, and that they obey a first-order auto-regressive (AR-1) process with the one-step correlation parameter $\alpha_{\delta p} = e^{-\pi B_{\delta p}\Delta t}$, where $B_{\delta p}$ is the 3 dB width of the p.s.d. of $\delta\tau_{p,i}$. Setting $\Delta f = f_1 - f_2$ and $\Delta t = t_1 - t_2$, we have

$$\begin{aligned} C_{\gamma_p}(\Delta f, \Delta t) &= E\{[\gamma_p(f_1,t_1) - \bar{\gamma}_p(f_1)][\gamma_p(f_2,t_2) - \bar{\gamma}_p(f_2)]^*\} \\ &= S_p e^{-\frac{(2\pi\Delta f)^2\sigma^2_{\delta p}}{2}} e^{-(1-\alpha_{\delta p})(2\pi f_1)(2\pi f_2)\sigma^2_{\delta p}} \\ &\quad \times [1 - \rho_p(\sqrt{2\alpha_{\delta p} f_1 f_2})] \\ &\approx \rho_p(\Delta f)\cdot e^{-\pi B_p(f_{1,2})\Delta t}\cdot 2\sigma_p(f_1)\sigma_p(f_2) \end{aligned} \quad (3)$$

where $B_p(f) = (2\pi f\sigma_{\delta p})^2 B_{\delta p}$ is the effective Doppler bandwidth and $f_{1,2}$ stands for either of the two frequencies f_1 or f_2. To simulate the effect of scattering, one can directly generate $\delta\tau_{p,i}$ as described above and use Eq. (1). Alternatively, a statistically equivalent AR-1 model is proposed [6] for $\mathbf{\Delta\gamma}_p[n] = [\Delta\gamma_p(f_0, t_0 + n\Delta t_s), \Delta\gamma_p(f_1, t_0 + n\Delta t_s), \ldots]^T$ where $\Delta\gamma_p(f,t) = \gamma_p(f,t) - \bar{\gamma}_p(f)$. Each realization $\mathbf{\Delta\gamma}_p[n]$ of the auto-regressive process is generated in one shot using a non-white noise whose frequency covariance function is defined to ensure the desired correlation properties of Eq. (3) for the resulting scattering coefficients.

Fig. 1 shows $C_{\gamma_p}(\Delta f, \Delta t)$ obtained for the special cases of $\Delta t = 0$ and $\Delta f = 0$ which indicate the frequency- and time-correlation functions, respectively. Shown in the figure are also the correlation functions of a simulated scattering process. The nominal channel geometry of the Kauai Acomms MURI (KAM'11) experiment is used for generating the simulated process. A complete description of the channel geometry and the types of signals used in this experiment will be presented

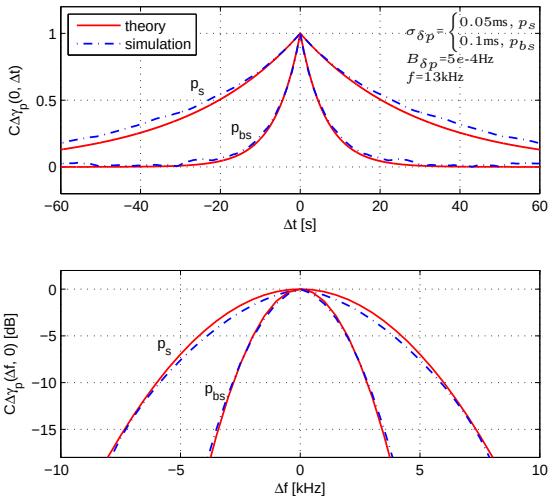

Fig. 1. Time (top) and frequency (bottom) correlation functions, obtained theoretically and via simulation for surface scattered (p_s) and bottom-surface (p_{bs}) paths.

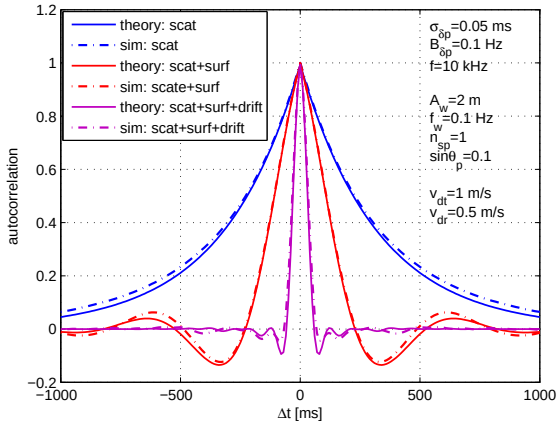

Fig. 2. Time-correlation of the small-scale coefficient $\tilde{\gamma}_p$ in the presence of surface and drifting motion.

in Section III. Here, our goal is to demonstrate the various correlation functions that statistically model the underwater channel and to verify that a channel simulated according to the proposed model conforms the theoretical correlation functions.

Motion of the transmitter/receiver and the reflection points, modeled by a Doppler scaling factor a_p, leads to additional variation that affects the small-scale coefficient as

$$\tilde{\gamma}_p(f,t) = \gamma_p(f,t) e^{j2\pi a_p f t} \quad (4)$$

Three types of motion are considered: (i) drifting or unintentional transmitter/receiver motion, (ii) vehicular or intentional transmitter/receiver motion, and (iii) surface motion caused by waves. The types of motion associated with the transmitter/receiver are described by the speed and the direction of movement. The surface at each reflection point is assumed to demonstrate a vertical oscillation that is modeled as sinusoidally varying in time, with amplitude A_w

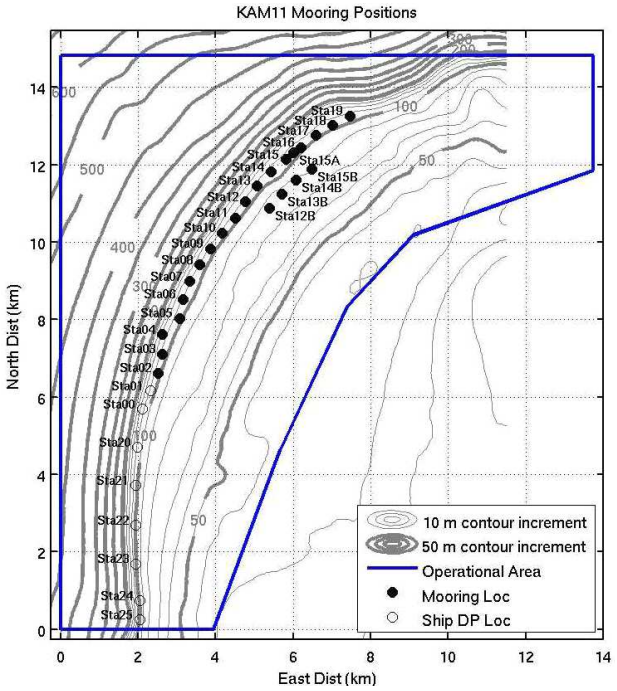

Fig. 3. Bathymetry map of KAM'11 experiment.

and frequency f_w. Assuming that the reflection points are sufficiently far apart, the phases at which different reflection points catch the surface are independent and hence modeled as uniformly distributed over 2π. The overall time-correlation function of the small-scale coefficient $\tilde{\gamma}_p(f,t)$ is shown to exhibit Bessel-like fluctuations [6]. Fig. 2 shows the time-correlation function corresponding to two different scenarios: when there is surface motion only, and when, in addition to the surface motion, the transmitter and the receiver drift at speeds v_{dt} and v_{dr}, respectively. The figure corresponds to the path with one surface reflection (n_{sp}=1) with a grazing angle (θ_p) of 0.1 radians. As the figure shows, additional motion narrows the correlation function, hence decreasing the coherence time. The figure also shows the estimated time-correlation functions for a channel simulated using the same parameters.

On the large scale, the variations of the system geometry, hence the multipath parameters h_p and τ_p, over longer periods of time are studied. These variations are believed to influence the SNR (or equivalently the channel gain) through its local average. For a system operating in the frequency range $[f_0, f_0 + B]$, the instantaneous channel gain is defined as

$$\tilde{G}(t) = \frac{1}{B}\int_{f_0}^{f_0+B} |H(f,t)|^2 df \tag{5}$$

whose local average, referred to as the gain, is obtained by averaging over the small-scale phenomena:

$$G = E_{\tilde{\gamma}}\left\{\tilde{G}(t)\right\} \tag{6}$$

We denote the gain in dB by $g = 10\log G$.

To complete the channel simulator, the large-scale variations of the channel geometry are treated as follows. The displacements of the transmitter/receiver/surface height, and the channel length around nominal values are modeled as Gaussian AR-1 processes. Using Bellhop, the path gains and delays are calculated for each realization of the channel geometry. Realizations of the channel geometry are separated by a time difference on the order of the coherence time of the large-scale processes ($\sim$1 minute) during which a set of small-scale channel data are generated.

III. Comparison with real data

In this section, we compare the statistical characteristics of a simulated channel with those of an experimental underwater acoustic channel. In addition, the performance of a communication system set up to operate on the simulated channel is compared with the performance of the same system operating on the experimentally recorded data. The experimental data are obtained from the KAM'11 experiment. The KAM'11 experiment was conducted in July 2011 off the coast of Kauai Island in Hawaii, in about 100 m deep water, as shown in the bathymetry map of Fig. 3.

A. Channel characteristics

For studying the channel characteristics, the data obtained from the Woods Hole Oceanographic Institution (WHOI) communication system were analyzed. This system, which is labeled in Fig. 3 as Sta03 (transmitter) and Sta09 (receiver), operated in the 8.5 kHz to 17.5 kHz bandwidth. Pseudo-noise (PN) sequences, BPSK modulated and repeatedly transmitted at rate 6.5 kbps were used for channel probing.

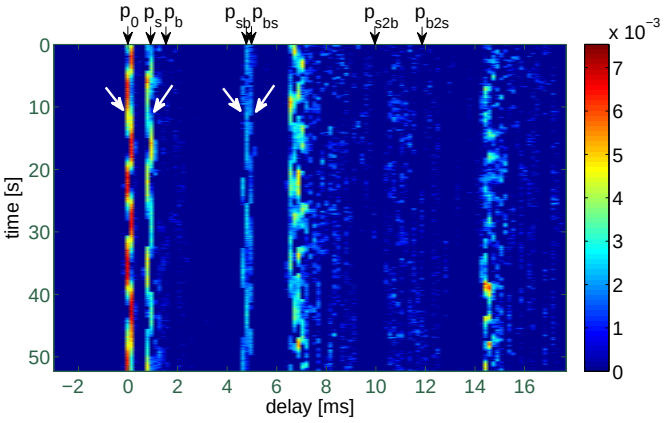

Fig. 4. Time-evolution of the magnitude baseband impulse response of the KAM'11 channel. Specified on top are the nominal path delays.

Assuming sinusoidally moving surface and transmitter/receiver drifting of several centimeters per second, an ensemble of small-scale coefficients $\tilde{\gamma}_p(f,t)$ is generated. The statistically equivalent model for $\mathbf{\Delta\gamma}_p[n]$ is used. The duration of the simulated data is set to one minute to match with the duration of the signals used in the KAM'11 experiment whose impulse response is shown in Fig. 4. The large-scale parameters are assumed to be fixed during this time interval. The

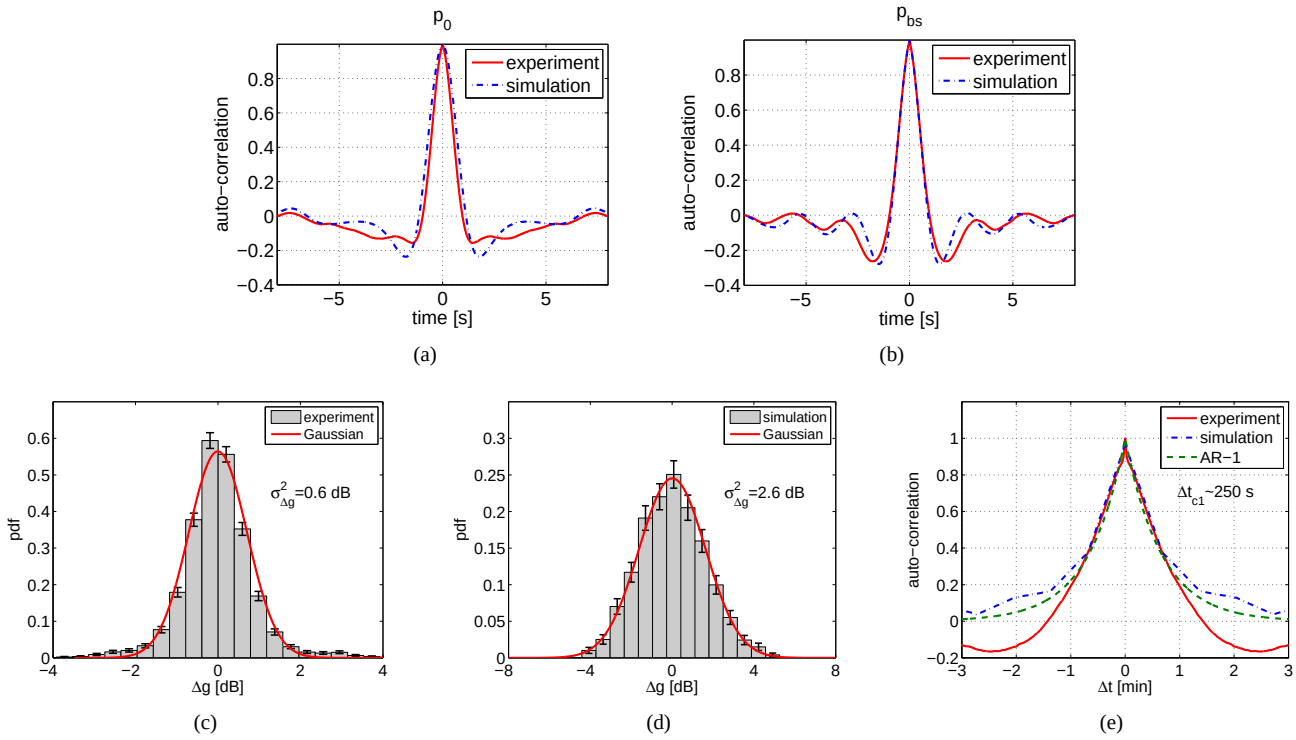

Fig. 5. Small-scale (top) and large-scale (bottom) statistics of the experimental and the simulated channels: time-correlation functions corresponding to (a) the direct path, and (b) the bottom-surface path; histogram of (c) experimental and (d) simulated gain and Gaussian approximation; (e) time-correlation of experimental and simulated gain and AR-1 auto-correlation.

simulated channel transfer function is formed using Eq. (2) and its inverse Fourier transform is used to obtain the time evolution of the path gains. The time-correlation properties of the simulated path gains are dictated by the variance $\sigma_{\delta p}^2$ and the Doppler spread $B_{\delta p}$ of the intra-path delays, as well as the motion-induced Doppler factors. Scattering occurs on spatial dimension on the order of the wavelength, which is 12 cm for the center frequency of our experimental system, and translates into a time variation of 0.07 ms. In the simulated channel, $\sigma_{\delta p}$ corresponding to the surface reflected path is set to 0.05 ms, and its value increases with the number of reflections for higher order paths (e.g. $\sigma_{\delta p}$=0.25 ms for the path with two surface and one bottom reflections).

From Eq. (3), the coherence time corresponding to the scattering process is inversely proportional to $B_{\delta p}$. If $B_{\delta p}$ is selected to be too high (i.e. more than 0.01 Hz), the coherence time of the path gains will become less than that observed in the experiment. On the contrary, if $B_{\delta p}$ is selected to be too low (i.e. less than 1e-4 Hz), the time-correlation functions will be almost flat for the duration of the simulated signal. We have selected $B_{\delta p}$=5e-4 Hz which is in between the two thresholds.

The periodic variations of the path delays about the nominal values in Fig. 4, are used to estimate the motion. We focus on paths p_0, p_s, p_{sb} and p_{bs}, marked on the figure by white arrows, which are observed around the nominal delays and are hence considered as valid paths. Since all paths, including the direct path, exhibit such delay variations, the effect of transducer motion seems to be more dominant than surface fluctuation. Vehicular motion is not considered because no average delay shift is observed. In order to calculate the transducer drifting, we model the delay fluctuations as a sinusoid of amplitude 160 microseconds (on the delay axis) and period 15 seconds (on the time axis), as observed in the figure. The derivative of this function yields the drifting Doppler factor, which is related to the relative speed, projected onto the path direction, by a factor of $1/c$, where c denotes the speed of sound in water. Assuming that all paths have approximately same angles of arrival (horizontal channel with range much greater than depth), a sinusoidal drifting speed of amplitude 10 centimeters per second and a period of 15 seconds results in the observed Doppler factor.

The sound speed profile was set based on measurements made during the experiment. The effect of temperature seemed to be the dominant factor as the measurements showed constant sound speed of about 1537 meters per second for up to 40 m depth which decreased to about 1530 meters per second at higher depths.

We test the accuracy of the simulator by comparing the statistics of the simulated and the experimental channels. Fig. 5 and Table I summarize the properties of the histograms and the time-correlation functions of the small-scale path gains and the large-scale channel gain, estimated from experimental and simulated data.

Table I lists the properties of the histograms of the path gains. The J-S divergence between the estimated histograms and the fitted distributions is listed in Table I as a quantitative

TABLE I
JENSEN-SHANNON DIVERGENCE FOR RICEAN FITS AND THE CORRESPONDING RICEAN K-FACTORS.

		p_0	p_s	p_{sb}	p_{bs}
JS divergence	experiment	5.1e-4	5.8e-3	5.8e-3	2.9e-3
	simulation	1.2e-3	4.7e-3	4.2e-3	3.5e-3
K-factor [dB]	experiment	22	15	12	9
	simulation	21	15	10	11

measure of the goodness of the fits. The negligible divergence indicates a good fit for all path gains, both for experimental and simulated channels. The Ricean K-factor is also listed in the table. Its value for the direct path (p_0) is greater than that of the other paths, indicating a stable arrival as there is no encounter with the surface.

Figs. 5(a) and (b) show the time domain auto-correlation functions of the direct and the bottom-surface reflected path coefficients, respectively. The correlation function corresponding to simulated data matches with that of the experimental data which approves the choice of the scattering and motion parameters used for simulation. Bessel-like auto-correlation functions caused by motion-induced Doppler are observed clearly for the bottom-surface-reflected path which undergoes higher Doppler distortion.

Figs. 5(c) and (d) show the histograms of the large-scale channel gain variation $\Delta g = g - \bar{g}$, where $\bar{g}$ denotes the average of g, estimated for experimental and simulated data, respectively. The data consisted of 585 minutes of transmission, over a duration of 130 hours (9 minutes every 2 hours). The figures also show the Gaussian fits. The 95% confidence intervals of the histogram bars are plotted. For almost every bar, the Gaussian fit falls inside the confidence interval which indicates the goodness of the fits. Finally, Fig. 5(e) shows the auto-correlation function of Δg estimated for simulated and experimental data along with the auto-correlation function of an AR-1 process. Both simulated and experimental gain seem to obey the AR-1 auto-correlation function especially for time differences of less than a minute.

B. System performance

The data used for evaluation of the system performance were obtained from Scripps Institute of Oceanography (SIO) transducers, which operated in the 20 to 32 kHz bandwidth, and are labeled in Fig. 3 as Sta02 (transmitter) and Sta08 (receiver). The transmitted signal consisted of consecutive OFDM blocks with a varying number of carriers. We compare the performance of coherent and differentially coherent receiver with and without partial-FFT (P-FFT) demodulation [7], [8]. P-FFT demodulation is a technique in which the received OFDM block is divided into P non-overlapping segments and FFT demodulation is applied on each segment separately. The outputs of the FFTs are weighted and combined. The combiner weights are optimized for each carrier, so as to approximate the effect of optimal (channel-matched) pre-FFT filtering.

Fig. 6 shows the average MSE performance result for the KAM'11 experiment, utilizing 8 receiver elements (separated by 7.5 meters). The figure demonstrates that in this experiment,

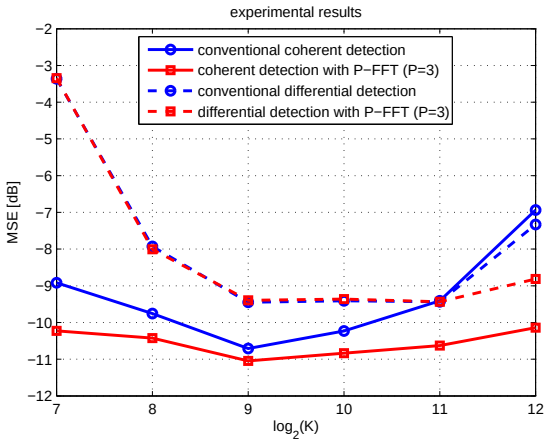

Fig. 6. Average MSE performance for the KAM'11 experiment. The average SNR is observed to be 15 dB at each receiver element within the signal bandwidth. Averaging is performed over 5×10^4 QPSk symbols which were transmitted in 3 frames separated by 3 hours.

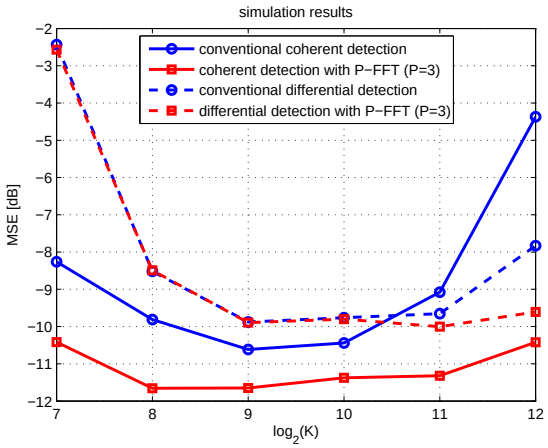

Fig. 7. Average MSE performance obtained via simulation. The simulated channel parameters are selected to match those of the experimental channel, observed for the experimental data as described in Sec. III-A, and similar receiver configurations are used. The MSE results demonstrate the same trend as those observed for the experimental data.

conventional differential detection is seen to be competitive to coherent detection for a large number of carriers (which coincides with high bandwidth efficiency). P-FFT further improves the performance of both techniques by reducing the inter-carrier interference which arises with a large number of carriers (long block duration makes the system more susceptible to the time-variation).

Fig. 7 provides MSE results for simulation, where the channel parameters are set as described in Sec. III-A. The characteristics of the noise measured during the experiment are shown in Fig. 8. This noise is observed to have Gaussian distribution and a relatively flat p.s.d. in the bandwidth of interest (20 kHz–32 kHz). The noise used in simulation was thus modeled as white Gaussian, and its power was set to yield the same SNR as the one observed in the experimental data (15 dB).

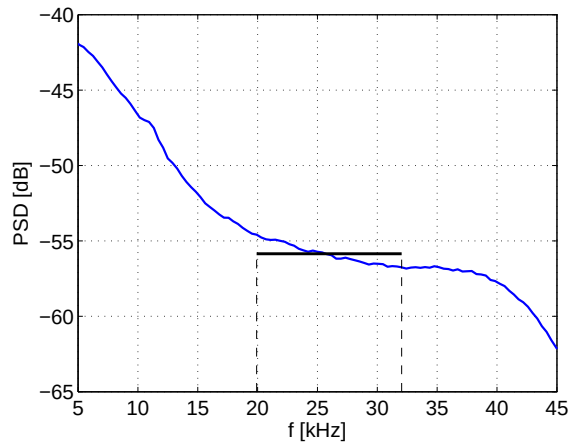

(a)

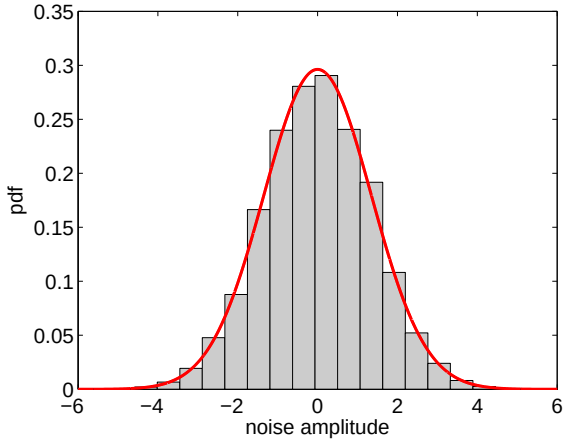

(b)

Fig. 8. Noise statistics, estimated from 120 seconds of recording of ambient noise during the experiment: (a) p.s.d., (b) p.d.f. The psd is obtained by the Welchs method, using an FFT of size 256 with 50% overlap.

Comparing the results of Figs. 6, 7, we see that the system performance obtained via simulation follows the same trend as that observed with real data. The discrepancies that occur affect the absolute values, but not the trend. For instance, the break-even point between the conventional coherent and differentially coherent detection occurs at 2048 carriers, after which differential detection outperforms coherent detection. This fact gives credibility to the proposed channel simulator, and indicates that it can indeed be used as a computationally-efficient tool for system optimization.

IV. Conclusions

A channel simulator was designed that takes into account the physical laws of acoustic propagation as well as the effects of small- and large- scale channel variations. Small-scale scattering components were modeled by complex Gaussian multiplicative coefficients with an exponentially decaying auto-correlation function which demonstrates Bessel-type fluctuations in the presence of motion-induced Doppler. Large-scale channel variations were modeled by log-normal channel gain whose temporal properties follow an AR-1 process. The simulator parameters were selected to match with the acoustic channel of the KAM'11 experiment, and a series of channel impulse responses were generated. The histograms and the time-correlation functions of the small-scale path coefficients and the large-scale channel gain were compared with those of the experiment, and matching results were observed. The simulated channel was used to convey an OFDM signal to coherent and differentially coherent detectors. The MSE performance of the experimental and the simulated channel were shown to be similar, indicating that the simulator can indeed be used for designing an optimized receiver.

Acknowledgements

This work was supported by the ONR MURI grant #N00014-07-1-0738, the ONR grant #N00014-09-1-0700, and the NSF grant #CNS-1212999.

References

[1] M. B. Porter, "Bellhop Code," [online]. Available: http://oalib.hlsresearch.com/Rays/index.html.

[2] R. M. Heitsenrether and M. Badiey, "Modeling Acoustic Signal Fluctuations Induced by Sea Surface Roughness," in Proc. *American Institute of Physics Conference*, 2004.

[3] B. Tomasi, G. Zappa, K. McCoy, P. Casari, and M. Zorzi, "Experimental Study of the Space-Time Properties of Acoustic Channels for Underwater Communications," in Proc. *IEEE Oceans Conf.*, 2010.

[4] J. C. Peterson and M. B. Porter, "Ray/Beam Tracing for Modeling the Effects of Ocean and Platform Dynamics," in Proc. *Underwater Communications: Channel Modelling & Validation*, Sestri Levante, Italy, Sep 2012.

[5] J. Llor, M. Stojanovic, and M. P. Malumbres, "A Simulation Analysis of Large Scale Path Loss in an Underwater Acoustic Network," in Proc. *IEEE Oceans Conf.*, 2011.

[6] P. Qarabaqi and M. Stojanovic, "Statistical Characterization of Underwater Acoustic Channels," submitted to *IEEE Journal of Oceanic Engineering, Special Issue: Underwater Communications*, Dec 2012.

[7] Y. Aval and M. Stojanovic, "A Method for Differentially Coherent Multichannel Processing of Acoustic OFDM Signals," in Proc. 7-th IEEE Sensor Array and Multichannel Signal Processing Workshop (SAM), Hoboken, NJ, June 2012

[8] Y. Aval and M. Stojanovic, "Partial FFT demodulation for Coherent Detection of OFDM Signals Over Underwater Acoustic Channels," in Proc. *IEEE Oceans Conf.*, 2013.